Computational and Theoretical Chemistry 1098 (2016) 41–49

Contents lists available at ScienceDirect

Computational and Theoretical Chemistry

journal homepage: www.elsevier.com/locate/comptc

Electric and structural properties of polymeric graphite carbon nitride (g-C_3N_4): A Density Functional Theory study

Alexander M. Silva [a], Mariana I. Rojas [b,*]

[a] Divisão de Metrologia de Materiais, (INMETRO) Instituto Nacional de Metrologia, Normalizacão e Qualidade Industrial, Duque de Caxias, Río de Janeiro, RJ 25245-020, Brazil
[b] INFIQC – Departamento de Matemática y Física, Facultad de Ciencias Químicas, Universidad Nacional de Córdoba – Ciudad Universitaria, 5000 Córdoba, Argentina

ARTICLE INFO

Article history:
Received 19 September 2016
Received in revised form 14 October 2016
Accepted 2 November 2016
Available online 3 November 2016

Keywords:
Graphite carbon nitride
Properties
Density Functional Theory calculation

ABSTRACT

Graphite carbon nitride (g-C_3N_4) is a new class of N-doped material that exists in 2D and 3D structures. They are nanoporous materials with multiple technological applications. That is why we present here a complete Density Functional Theory study about the properties of (2D) sheets: triazine and tri-s-triazine and the (3D) crystals. The layers can be stacked in different forms on the crystals. Thus, we consider different stacking types and calculate the adhesion energy between the layers. We also simulate the X-ray diffraction pattern (XRD) and Transmission Electron Microscopy (TEM) pattern using the optimized geometries, because all these data are useful for experimentalists. As g-C_3N_4 is an organic semiconductor, we inform the electrical properties for sheets and crystals. We perform band diagrams using symmetry paths in the Brillouin zone (BZ) and Density of States (DOS) calculations. We compare graphene and graphite materials with 2D and 3D g-C_3N_4 structures, because they are a good reference as they are well known.

1. Introduction

Binary nitrogen and carbon materials are a new variety of carbonaceous materials doped with nitrogen. Since C and N are the most abundant elements in our planet, these covalent solids are environment friendly. They can be produced at large scales with low cost by polymeric condensation of N-rich precursors. At ambient conditions, g-C_3N_4 is the most stable allotrope of the carbon nitrides (C_3N_4) [1].

Due to the N content in 2D sheets of g-C_3N_4, there is a periodic distribution of pores. According to their distribution, there are two different allotropic structures: triazine and tri-s-triazine. The second structure was identified by Schinck [2], by means of solid state NMR studies. Kroke [3] found that this structure is 30 kJ/mol more stable than triazine by means of DFT calculations.

3D crystals of g-C_3N_4, are formed by stacking of sheets in different forms [4]. Despite the presence of pores, due to the binary composition of aromatic sheets, they are bonded through Van der Waals interactions and are expected to have greater adhesion strength than those observed between graphene sheets forming the structure of graphite [5].

By means of DFT calculations, Teter [6] studied the different allotropic forms of C_3N_4. About triazine, they found that the layers are stacked on AB type with a unit cell of 14 atoms. This crystal has $P\bar{6}m2$ symmetry.

Triazine and tri-s-triazine 2D sheets can be obtained by treating the material with strong acids. N atoms are protonated charging the sheets positively so they repel each other, giving the chemical exfoliation.

These sheets have semiconductor's properties with a greater band gap than graphene, which has a small gap of 0.05 eV. Thus, these layers allow their use in devices of high speed switching [7]. 3D crystals of g-C_3N_4, like graphite, are also semiconductors. In the case of 3D crystals of g-C_3N_4, the band gaps are even greater than those of the respective sheets.

As g-C_3N_4 is a semiconductor, it adsorbs photons of light that are in the UV/visible range of the electromagnetic spectrum, which allows its application in photocatalysis and photoelectrochemical devices, like efficient and cheap solar cells, in the construction of LED, and in the catalysis under UV and visible light [8–10].

Moreover, g-C_3N_4 is a nanoporous material of low density. This property makes it a possible candidate to safely store hydrogen. This application is important to solve the problem of using hydrogen as a clean fuel for vehicle use [11].g-C_3N_4 with graphite oxide nanohybrid are employed in the construction of anode of lithium ion batteries, because they exhibit an unprecedented high, stable

* Corresponding author.
E-mail address: mrojas@fcq.unc.edu.ar (M.I. Rojas).

http://dx.doi.org/10.1016/j.comptc.2016.11.004
2210-271X/

and reversible capacity of 1525 mA h/g at a current density of 100 mA/g after 50 cycles, suggesting to be remarkably promising candidates for energy storage [12–15].

As these 3D materials have high electrocatalytic activity, they can be used in the manufacture of biosensors and biomedical devices. These sensors are employed in electrochemistry, which is a promising tool, due to the high sensitivity, good selectivity and ease operation [10].

In the present work we make a comparative study about geometrical and electrical properties of triazine and tri-s-triazine sheets as well as crystals with the well-known graphene and graphite materials. We investigate the structural properties, propose different type of stacking and calculate the adhesion energy between layers. This allows knowing if the material can be mechanically exfoliated. We simulate the XRD and TEM patterns and study the electrical properties of sheets and crystals.

2. Model and computations

The optimized lattice parameters for the 2D sheets of graphene, triazine and tris-s-triazine are 2.46 Å; 4.80 Å and 7.20 Å, respectively.

All DFT calculations are performed using the Quantum Espresso package [16] with Van der Waals interactions. The Kohn-Sham orbitals and charge density are expanded in plane-waves basis sets up to a Kinetic Energy cutoff of 60 and 480 Ry for all atoms. Ultra soft pseudopotentials are employed with the Perdew-Burker-Ernzerhof (PBE) approximation for exchange and correlation in the functional [17,18]. The BZ is sampled with $12 \times 12 \times 1$ or $12 \times 12 \times 12$ irreducible Monkhorst-Pack k-point grid [19] for the 2D and 3D systems, respectively.

The convergence threshold for the total energy at each electronic calculation is set to 1×10^{-8} *Ry*. Geometry optimizations are performed employing the Broyden-Fletcher-Goldfarb-Shanno (BFGS) algorithm (for stress minimization) and total forces acting on each ion are minimized to reach less than 1×10^{-3} Ry/a.u. by movement of the ionic positions.

3. Results and discussion

3.1. 2D Sheets

Fig. 1 shows a 2D graphene sheet, which is a 2D covalent solid with a honeycomb type structure. The unit cell is a hexagonal lattice with a base of two C atoms. The layer is perfect. Each C atom has the same environment. The distance between C atoms is 1.42 Å and they form angles of 120°, which are characteristic of the sp^2 hybridization. None of the C atoms is charged since the sheet is composed of one type of atom. In order to study the electric properties, we calculate the symmetry path through $\Gamma \rightarrow K \rightarrow L \rightarrow \Gamma$ points of the BZ. The band diagram is also shown in Fig. 1, together with the density of states (DOS). The maximum of the valence band (MBV) and the minimum of the conduction band (mBC) are on the K-point, giving a narrow band gap (ΔE_g) of 0.05 eV. It can be said that it is a zero-gap semiconductor because its conduction and valence bands meet at the Dirac points [20].

Fig. 1 shows triazine and tri-s-triazine 2D sheets which are the allotropes of g-C_3N_4. They are binary covalent solids, which are composed by C and N atoms, arranged in a different order. C and N atoms are bonded by polar covalent bonds. These sheets have a distribution of charge because they have different electronegativities.

Triazine has also a hexagonal lattice with a 7 atom base per unit cell. There is a periodic distribution of pores, due to the different coordination of the N atom.

Analyzing the structure of the sheet, we find three equivalent C atoms, with an atomic charge of −0.378 atomic units (a.u.). Fig. 2 shows the two types of N atoms: N1 with two C neighbors. There are three N1 atoms in the base. They belong to the aromatic ring and have a charge of 0.253 a.u. The interatomic distance $d_{C\text{-}N}$ is equal to 1.33 Å. The second type is N2 atom, with three C neighbors. There is only one N2 atom in the base which connects the aromatic rings. It has a charge of 0.376 a.u. and greater interatomic distance of 1.46 Å, since it forms single bonds with C atoms of three different rings. The angles are not exactly of 120 degrees, indicating that there are distortions in the sp^2 hybridization. The geometric data descriptions are listed in Table 1.

Fig. 3 compares the Partial Density of States (PDOS) of C atom in the graphene sheet with C in the triazine sheet. In the second case, the bands are shifted to the left and are of greater intensity, due to the atoms are negatively charged. The total PDOS peak at −8 eV comes from the superposition of the $2p_x$ and $2p_y$ bands, and the peak at −4.5 eV is due to the $2p_z$ bands. Although the 2s, $2p_x$ and $2p_y$ bands are shifted to lower energy, all of them are in the same energy region, allowing the sp^2 hybridization.

Fig. 4 shows the PDOS of the two types of N atoms. Here, there is not a reference structure where the N atom appears uncharged. The N2 atom has a greater positive charge than the N1. N2 peaks corresponding to the 2s and $2p_x$ bands are of less density and form three σ-bonds with an interatomic distance of 1.46 Å with each of the three neighboring C atoms by means of the 2p orbitals. The N1 atom belongs to the aromatic ring, while the N2 atom connects the rings by means of a single bond.

In order to study the electric properties of the triazine sheet, we calculate a symmetry path in the BZ. Fig. 1 shows the band diagram and the DOS plot. From the DOS plot, it can be clearly seen that this material has a greater ΔE_g than graphene. It is equal to 1.25 eV and the Fermi level is close to the conduction band, so it is a semiconductor type n. As both MBV and mBC occur at the same point in the k-space, the Γ-point, it is possible to determine experimentally ΔE_g from the optical threshold. Due to this, direct transition occurs under light adsorption [21,22]. The relationship between ΔE_g and the threshold frequency (ν_g) is given by the following equation:

$$\Delta E_g = h\nu_g \tag{1}$$

The threshold wavelength (λ_g) can be obtained from:

$$\lambda_g = c/\nu_g \tag{2}$$

where c is the light speed. For a ΔE_g of 1.25 eV, the ν_g is 3.0×10^{14} Hz and λ_g is 992.6 nm (near infrared). All these data are listed in Table 2.

Tri-s-triazine has a hexagonal lattice with a base of 14 atoms per cell unit. In this lattice, the pores are greater than in the triazine case. There are two types of C atoms: (three) C1 and (three) C2 atoms, both binding with three N neighbors. The eight N atoms of the base are of three types: (six) N1 atoms with two C neighbors, (one) N2 and (one) N3 with three C neighbors. The locations of these atoms are shown in Fig. 2.

The C1 atom has a charge of −0.321 a.u. and it is bonded to two N1 atoms and one N3 atom. The C1 forms aromatics bonds (σ-bonds and π-bonds) with the two N1 neighbors by means of the $2sp^2$ hybridization and single bond with N3 atom. The interatomic distance of the double and single bonds are 1.33 Å and 1.48 Å, respectively. The C2 atom forms aromatic bonds with the two N1 neighbors by means of the $2sp^2$ hybridization and single bond with N2 atom. The interatomic distance of the double and single bonds are 1.33 Å and 1.39 Å, respectively. The angles are close to ∼120°, indicating a small distortion with respect to the sp^2 hybridization. All these data are listed in Table 1.

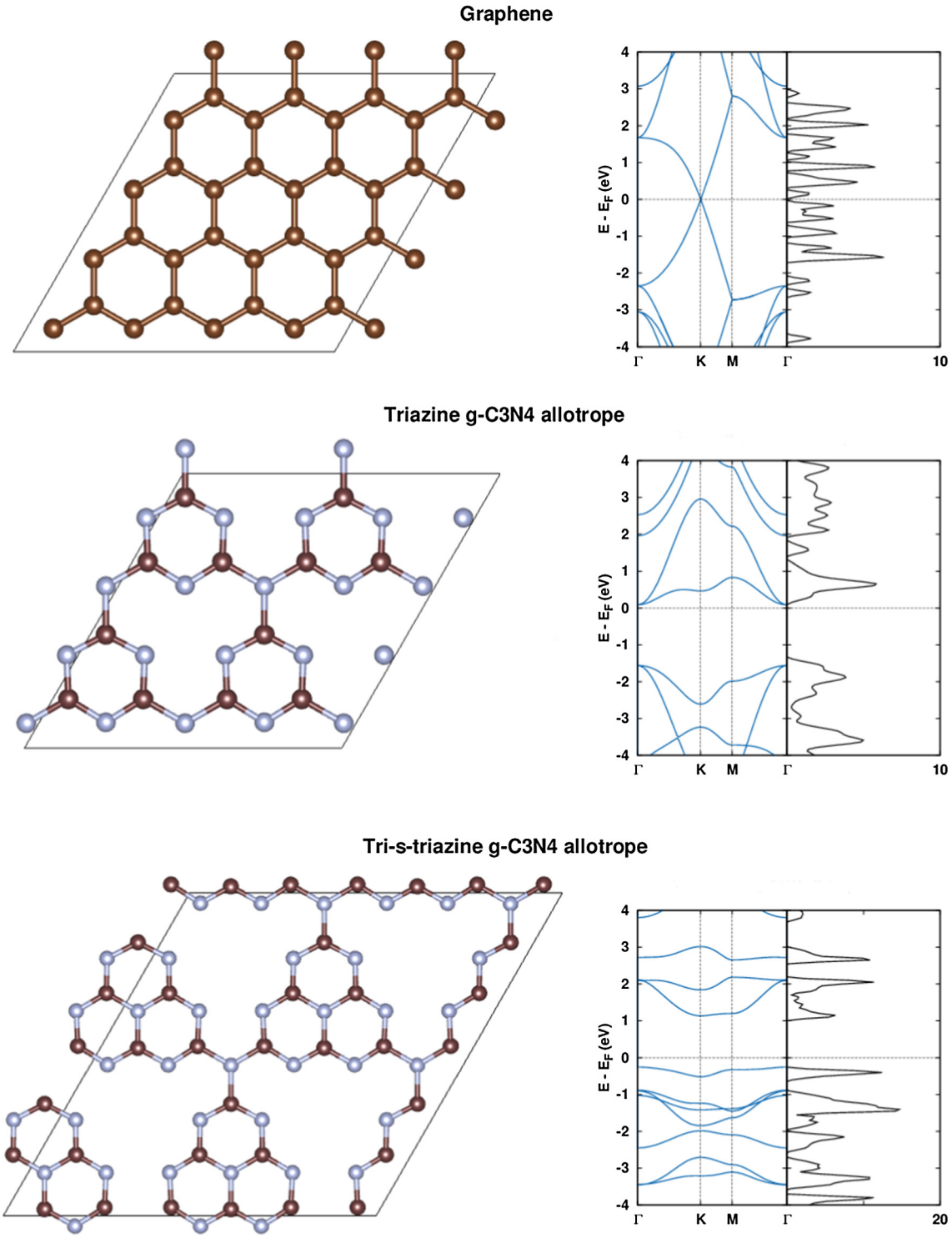

Fig. 1. 2D layers geometries, Band structure diagram and DOS corresponding (top) graphene; (medium) triazine; (down) tri-s-triazine. Brown and grey sphere represent C and N atoms, respectively. (For interpretation of the references to color in this figure legend, the reader is referred to the web version of this article.)

Fig. 5 shows the C1 and C2 bands of the tri-s-triazine sheet. As both types of atoms are charged negatively, their bands appear shifted to the left respect to the carbon neutral.

The C1 2s; $2p_x$ and $2p_y$ bands appear in the same interval of energy allowing the $2sp^2$ hybridization and the $2p_z$ form π-bond with N1 atoms.

Fig. 6 shows PDOS of N1; N2 and N3 atoms. The N1 atom has a charge of 0.233 a.u. It forms σ and π bonds with C1 atoms. The N3 atom has a charge of 0.469 a.u., which forms three single bonds with C1 atoms. The C2 atom has a charge of −0.415 a.u. It forms σ and π bonds with N1 atoms and form a single bond with N2 atom.

This sheet has the greatest ΔE_g. It is equal to 1.40 eV. Here the Fermi level is close to the valence band, so it is a semiconductor type p. as MBV is at Γ-point and mBC is at K-point. As the minima and maximum occur at different points in k-space, then, for the

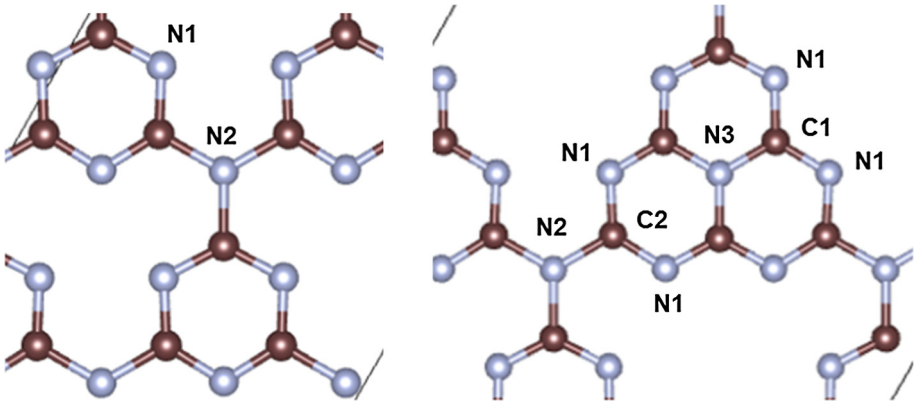

Fig. 2. The different types of C and N atoms in the (left) triazine and (right) tri-s-triazine sheets.

Table 1
2D-sheets geometric structure deta. Q_C and Q_N are the charges on C and N atoms in a.u.; $d_{C\text{-}C}$ and $d_{C\text{-}N}$ are the interatomic distances in Å; $\boldsymbol{C-\widehat{N}-C}$; and $\boldsymbol{N-\widehat{C}-N}$ are the angles in degrees.

2D sheet	Q_C		$d_{C\text{-}C}$	$\boldsymbol{C-\widehat{C}-C}$	
Graphene	0.00		1.42	120°	
2D sheet	Q_C	Q_N	$d_{C\text{-}N}$	$\boldsymbol{C-\widehat{N}-C}$	$\boldsymbol{N-\widehat{C}-N}$
Triazine	−0.378	0.253	1.33	124°	116°
		0.376	1.46	118°	118°
Tri-s-triazine	−0.321	0.233	1.33	119°	
		0.469	1.39	120°	125°
	−0.415	0.337	1.48	120°	118°

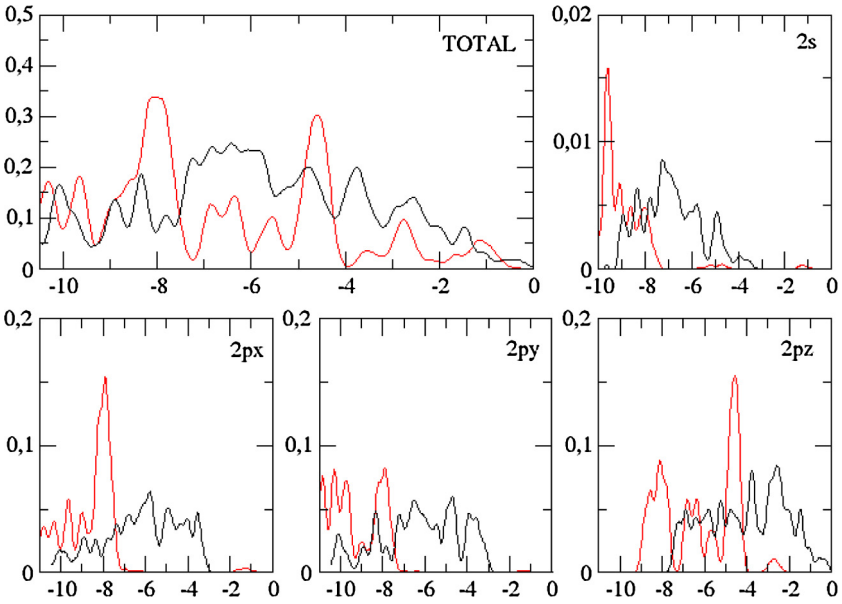

Fig. 3. PDOS of the graphene and triazine 2D sheets. (red line) C of the triazine and (black line) C of the graphene sheet. (For interpretation of the references to color in this figure legend, the reader is referred to the web version of this article.)

crystal momentum to be conserved, a phonon must also participate in the process. This type of excitation is known as indirect transition [21,22]. In this case, the energy of the photon absorbed ($h\nu_g$) is equal to:

$$h\nu_g = \Delta E_g + h\Omega \tag{3}$$

where Ω is the phonon frequency to conserve the momentum.

The phonon energy ($h\Omega$) is ~0.01 to 0.03 eV^0, much lower than the ΔE_g = 1.40 eV, so it is possible to approximate the v_g from the optical threshold: $\sim 3.4 \times 10^{14}$ Hz and $\lambda_g \sim 886.2$ nm (near infrared), respectively.

3.2. 3D crystals

In the previous section we describe 2D sheets. Now, we are interested in the description of the stacking to form 3D crystals.

Fig. 7 shows graphite with AB stacking which is the most stable one [23].

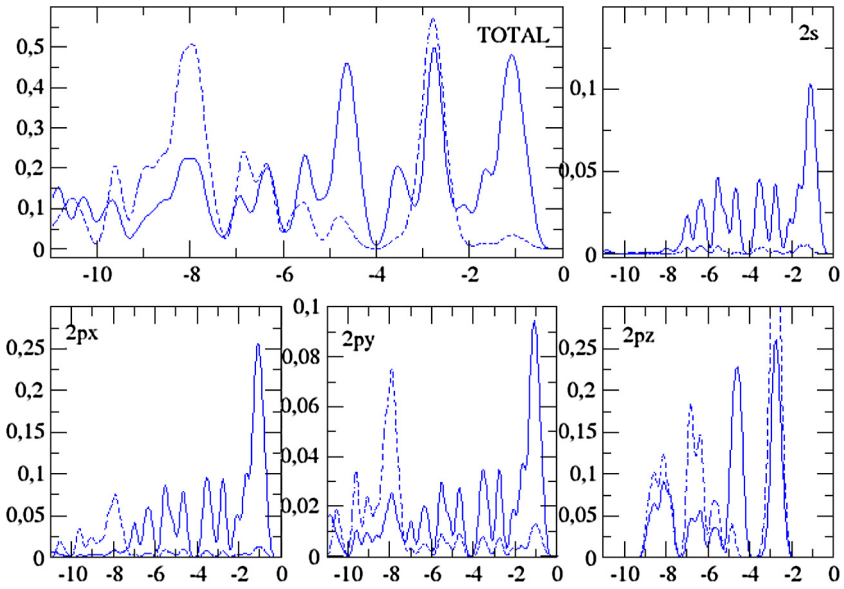

Fig. 4. PDOS of the 2D triazine sheet. (solid blue line) N-type-1 and (dashed blue line) N-type-2. (For interpretation of the references to color in this figure legend, the reader is referred to the web version of this article.)

Table 2
2D sheet properties at 0 K: type of semiconductor, Band gap, threshold frequency and threshold wavelength.

Structure	Type	ΔE_g [eV]	v_g [Hz]	λ_g [nm]
Graphene	–	0.05	–	–
Triazine	n	1.25	3.0×10^{14}	992.6
Tri-s-triazine	p	1.40	$\sim 3.4 \times 10^{14}$	~886.2

In order to evaluate the structural stability of the stacking patterns, we calculate the binding energy (E_b) as:

$$E_b = E_{3D} - n \cdot E_{2D} \quad (4)$$

where E_{3D} is the energy of the 3D crystal containing n sheets with periodic boundary condition in 3D and E_{2D} is the energy of the sheet in vacuum.

As the layers are bonded by Van der Waals forces, a measurable magnitude of the strength between sheets is the adhesion energy (E_{ad}), which can be calculated as follow:

$$E_{ad} = (E_b/(2 \cdot S)) \quad (5)$$

This is half of the E_b divided by the area (S) in contact.

The E_{ad} is an important magnitude, since it brings information about the aging of the material applied in technological devices when exposed to processes that could lead to mechanical exfoliation (i.e. the charge/discharge lithium ion in a rechargeable battery or loading/unloading of hydrogen for storage purposes).

We obtain for graphite E_{ad} equal to -0.31 J/m^2 that agrees with the value reported by Huang [5]. Since graphite has small adhesion energy, Geim and Novoselov can synthesize graphene by mechanical exfoliation, employing the Scotch tape method [20].

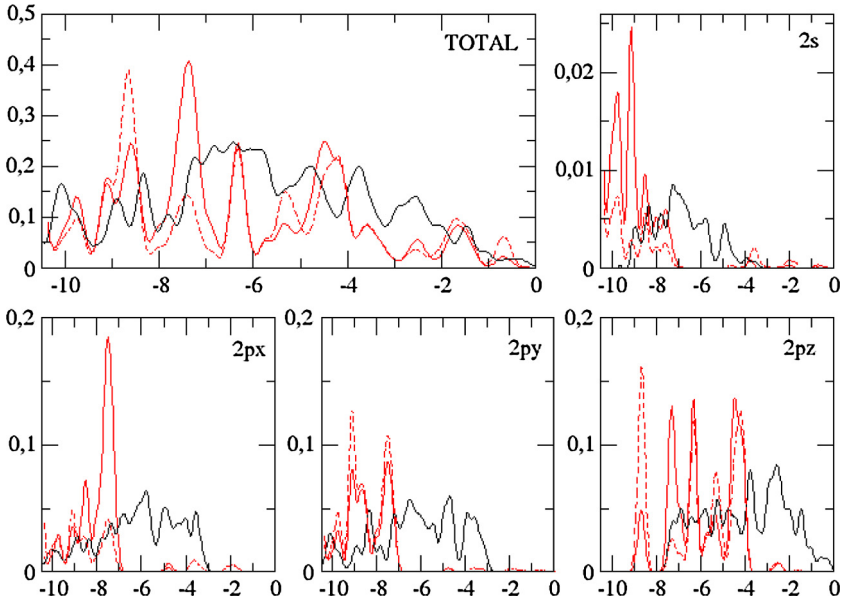

Fig. 5. PDOS of the graphene and tri-s-triazine 2D sheets. (solid red line) C1; (dashed red line) C2 of the tri-s-triazine and (black line) C of the graphene sheet. (For interpretation of the references to color in this figure legend, the reader is referred to the web version of this article.)

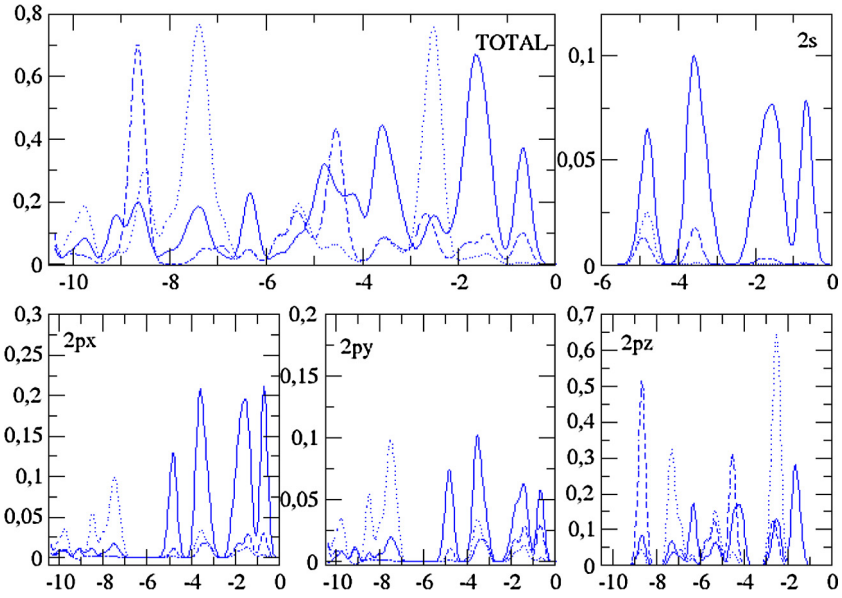

Fig. 6. PDOS of the 2D tri-s-triazine sheet. (solid blue line) N1; (dashed blue line) N2 and (dotted blue line) N3. (For interpretation of the references to color in this figure legend, the reader is referred to the web version of this article.)

The distance between sheets (d) obtained is equal to 3.24 Å that is close to the experimental value of 3.35 Å [24,25]. In Table 3, the values of binding energy (E_b), adhesion energy (E_{ad}) and interatomic distance (d) are listed.

Triazine and tri-s-triazine have shorter interplanar distances between 3.07 Å and 3.23 Å. They are enough to allow ion or gas storage. The adhesion energy is between -0.28 J/m^2 and -0.67 J/m^2, generally greater than graphite. Although these materials can mechanically exfoliate, they present a slower aging when they are used in diverse devices.

In the case of tri-s-triazine, we consider two different stackings, s1 and s2. The first one, stacking s1, the layers are displaced between them, a distance of 3.15 Å in y-direction. The second one, stacking s2, the layer are rotated 180° between them, so that the N atoms of consecutive layers, are facing. The most stable of the two is s1 since it presents the highest binding energy but both types can occur [6,26].

Another interesting property for the applications of these materials in the ion or gas storage is the porosity. We can study the porosity by means of the CrystalMaker© program [27].

The physical volume (V) of the simulation box was calculated as follows:

$$V = d \times S \tag{6}$$

where d is the interatomic distance and S is the area of the unit cell. The total filled (V_f) and void (V_v) spaces of the simulation box for the different materials are listed in Table 4. The V_v is theoretical accessible volume for ion or hydrogen storage. As expected, the most porous material is tri-s-triazine s2.

The graphite symmetry path in the BZ shows a narrow band gap of 0.15 eV, greater than the graphene sheet. In the graphite, the Fermi level is in the middle of the gap; it is equidistant to both bands. The MBV and mBC are at the same point of the k-space, the point K, so $\Delta E_{g,}$ is a direct gap.

Triazine and tri-s-triazine are both n-type semiconductors because the Fermi level is close to the conduction band. Triazine has a direct band gap of 1.35 eV, while tri-s-triazine has an indirect band gap of 1.90 eV. This can be clearly seen in Fig. 7. In the case of triazine, the minimum and maximum of the bands are located in the same k-point, the Γ one. While in the tri-s-triazine case, they are located in two different k-points, K and Γ points, respectively.

All these information, along with the optical properties, are listed in Table 5.

The interlayer distance can be experimentally measured by XRD. The angles at which the diffraction peaks appear following the Bragg's Law:

$$n\lambda = 2 \cdot d \cdot \sin(\theta) \tag{7}$$

where λ is the wavelength of the XRD and d is the interlayer distance.

In the XRD simulations, the geometries of the crystals are previously optimized by means of DFT calculations. The XRD patterns are simulated using the CrystalDiffract© program [28].

Fig. 8 shows Transmission Electron Microscopy (TEM) and XRD patterns simulated with the SingleCrystal© and CrystalDiffract© programs [28,29], respectively.

All the TEM patterns are different. This technique allows a unique identification of the structures.

The TEM graphite pattern shows a brilliant central spot at 000 surrounded by the six nearer neighbor spots of less intensity in the $2\bar{1}0$; 210; 020; $\bar{2}10$; $\bar{2}\bar{1}0$; $0\bar{2}0$ directions. The six second neighbor spots are of greater intensity than the first ones. The pattern shows the hexagonal symmetry characteristic of graphite with AB stacking.

Triazine also presents a hexagonal symmetry. The central spot is always the one of greatest intensity. The following points of greater intensity appear in the $\bar{2}\bar{4}0$; $2\bar{2}0$; 420; 240; $\bar{2}20$; $4\bar{2}0$ directions.

Tri-s-triazine s1 presents the central spot and the following six neighbors of greater intensity describe a rhombus with the 300; 330; $\bar{3}30$; $\bar{3}00$; $\bar{3}\bar{3}0$; $3\bar{3}0$ patterns. This structure has AB stacking but sheets are rotated 180° between them.

Tri-s-triazine s2 also exhibits hexagonal symmetry. The six spots of greater intensity that follow the central one are: $0\bar{3}0$; 300; 330; 030; $\bar{3}00$; $\bar{3}\bar{3}0$ patterns.

However, it is more familiar among experimentalists to analyze the XRD pattern, as they provide further information about the crystallinity of the material.

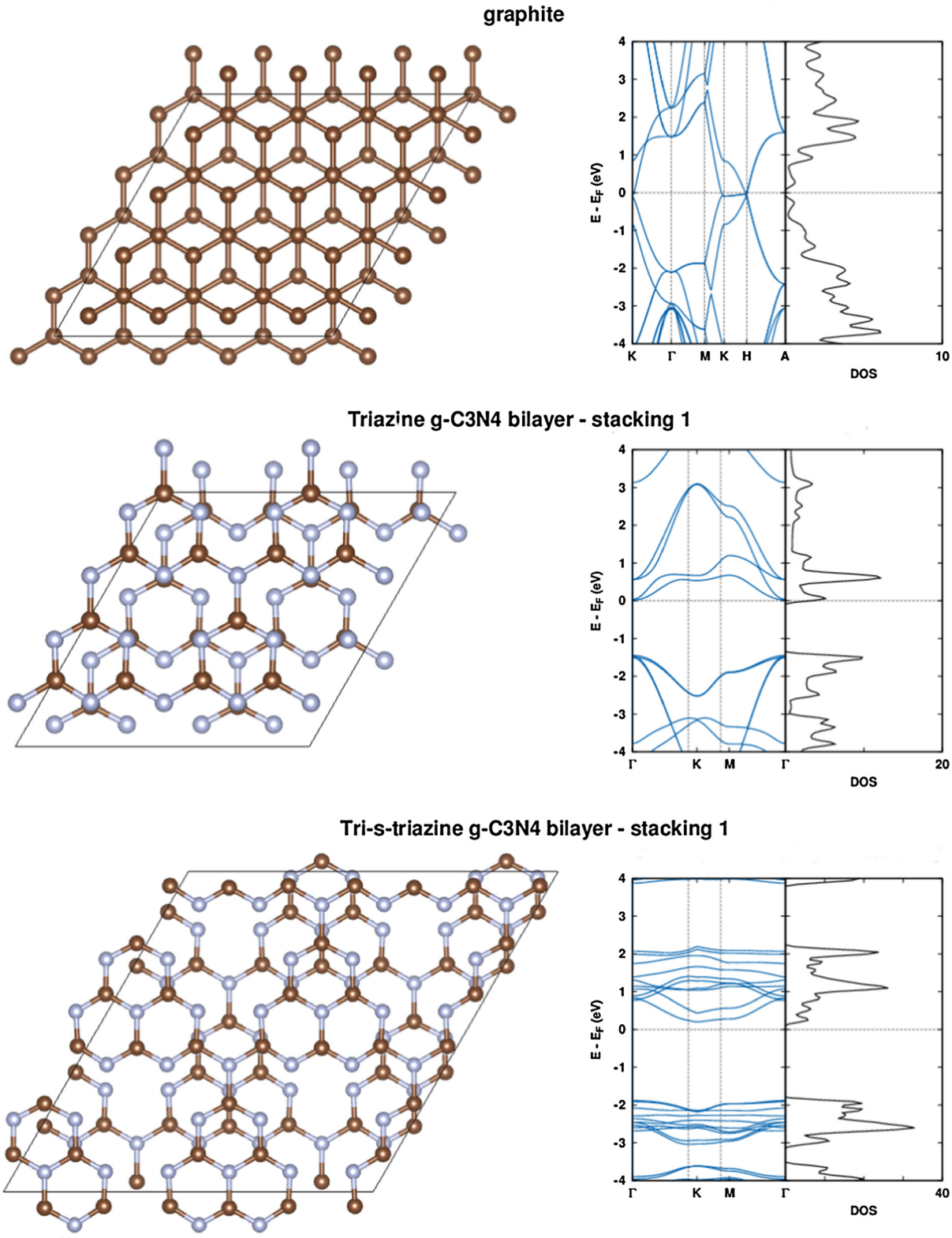

Fig. 7. 3D layers geometries, Band structure diagram and DOS corresponding (top) graphite; (medium) triazine; (down) tri-s-triazine. Brown and grey sphere represent C and N atoms, respectively. (For interpretation of the references to color in this figure legend, the reader is referred to the web version of this article.)

The parameters employed in the XRD simulations are: wavelength $K\alpha_1 = 1.54050$ Å and $K\alpha_2 = 1.54434$ Å; intensity ratio $I_1/I_2 = 2$; time of flight 89.954°; energy dispersive 4°; path length 100 m and a broadening of 0.2°.

The 002 peaks indicate the interatomic distance. They appear at 26.4°, 28.4°, 28.2°, 26.8° for graphite, triazine, s1 tri-s-triazine and s2 tri-s-triazine, and correspond to 3.24 Å; 3.07 Å; 3.07 Å; 3.23 Å, respectively. The more relevant peaks of hkl index corresponding to each structure are listed in Table 6.

In tri-s-triazine, the 100 peak appears at 13.6° for s1 case and at 13.5° for s2 case, while in the triazine, at this low angle, the 100 peak is not observed. Moreover, the peak 002 allows us to differen-

Table 3
Binding energies (E_b); interplanar distances (d); adhesion energies (E_{ad}) of the crystal studied.

Structure	E_b [eV]	d [Å]	E_{ad} [J/m^2]
Graphite	−0.82	3.24	−0.31
Triazine	−0.69	3.08	−0.28
Tri-s-triazine	−1.66	3.07	−0.67 s1
	−1.21	3.23	−0.49 s2

Table 4
Parameters to understand the porosity of the 3D crystals: filled space (V_f); void space (V_v) and total volume (V).

Structure		d [Å]	V_f [%]	V_v [%]	V [Å^3]
Graphito		3.24	15.3	84.7	141.5
Triazine		3.08	13.1	86.9	121.5
Tri-s-triazine	s1	3.07	11.7	88.3	269.8
	s2	3.23	11.2	88.8	283.6

Table 5
3D crystals properties at 0 K: type of semiconductor; Band gap; threshold frequency and threshold wavelength.

Structure	Type	ΔE_g [eV]	ν_g [Hz]	λ_g [nm]
Graphito	–	0.15	3.6×10^{13}	8271.4
Triazine	n	1.35	3.3×10^{14}	919.0
Tri-s-triazine	n	1.90	$\sim 3.0 \times 10^{14}$	~653.0

tiate between the different stackings of the tri-s-triazine. As the 002 peak appears at 28.3 for the s1 case and it is shifted to 26.8° for the s2 case. The peak 021 for the s1 is of greater intensity than that of the s2.

Table 6
Simulated X-ray diffraction pattern for graphite and the different g-C_3N_4 allotrope studied.

3D crystals	hkl	2Θ [°]	d [Å]
Graphite	002	26.4	3.24
	021	44.3	2.03
Triazine	110	20.8	4.28
	011	25.3	3.52
	002	28.3	3.08
	021	45.6	1.96
Tri-s-triazine s1	100	13.5	6.17
	101	19.6	4.35
	002	28.3	3.07
	021	31.6	2.75
Tri-s-triazine s2	100	13.6	6.52
	01$\bar{1}$	19.1	4.66
	002	26.8	3.23

4. Conclusions

A comprehensive and comparative DFT study about the structural and electronic properties of 2D and 3D g-C_3N_4 materials with respect to the (2D) graphene and (3D) graphite materials was performed.

The 2D triazine and tri-s-triazine sheets are nanoporous materials with a periodic distribution of porous.

Although they are semiconductors as the graphene sheet, these binary materials have higher bandgaps: 1.25 and 1.40 eV, respectively. In the case of triazine, it is a semiconductor type-n, while tri-s-triazine is type-p.

In the construction of 3D crystals we studied the stacking of the layer to form those crystals. We found only one type of stacking for

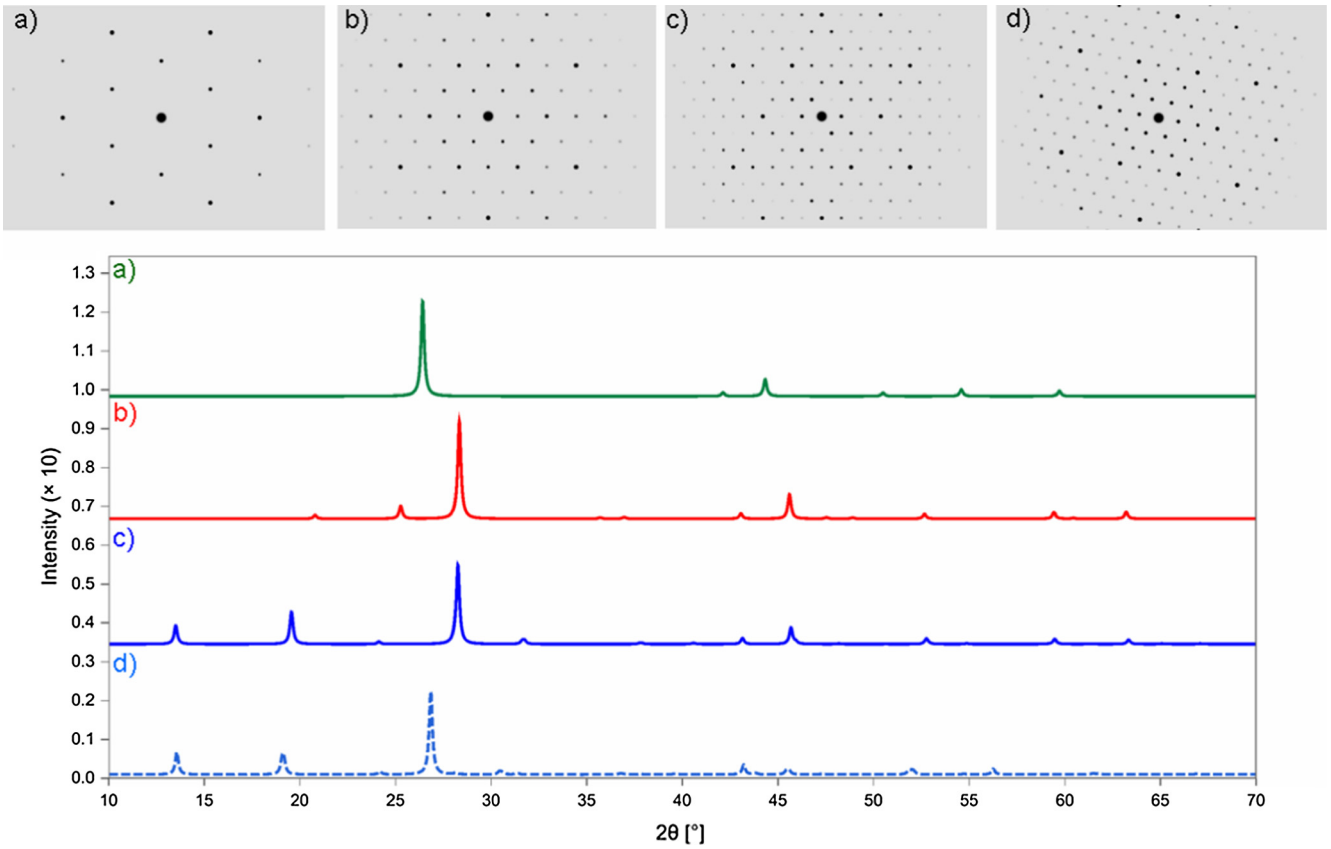

Fig. 8. Simulated TEM and X-ray diffraction patterns. (a) graphite; (b) triazine; (c) tri-s-triazine s.1; (d) tri-s-triazine s.2.

(3D) triazine, the AB one. In the (3D) tri-s-triazine case, we found two possible stackings; the most stable is s1.

In the XRD patterns, the 2Θ angles corresponding to 002 peaks of the graphite appear at 26.4° while those of g-C_3N_4 appear between 26.8° and 28.3°, which correspond to interplanar distances between 3.07 Å and 3.23 Å. Although these interplanar distances are shorter than the graphite one, they are enough to allow ion or gas storage. On the other hand, g-C_3N_4 crystals are more porous than graphite. Tri-s-triazine s2 is the most porous of the materials studied.

The adhesion energies of these materials are in the range −0.28 and −0.67 J/m^2, so they present slower aging than graphite, which has adhesion energy of −0.31 J/m^2.

According to their electrical properties, g-C_3N_4 materials are organic semiconductors with gaps of1.25 and 1.40 eV in the case of 2D sheets and 1.35 and 1.90 eV in the case of 3D crystals, so they can be employed in photochemical applications.

We believe that all this theoretical information could be of great value as well as helpful to experimentalists due to the numerous technological applications of these amazing materials.

Conflict of interest

The authors declare no competing financial interest.

Acknowledgment

This work was supported by PIP 11220120100031CONICET and SECyT Universidad Nacional de Córdoba. A.M. Silva wishes to thank INMETRO for a postdoctoral fellowship. The authors also wish to thank language assistance by Mrs. M.J. Martinez.

References

[1] A. Thomas, A. Fischer, F. Goettmann, M. Antonietti, J. Oliver Müller, R. Schlögl, J. M. Carlsson, Graphitic carbon nitride materials: variation of structure and morphology and their use as metal-free catalysts, J. Mater. Chem. 18 (2008) 4893–4908.
[2] B. Jürgens, E. Irran, J. Senker, P. Kroll, H. Müller, W. Schnick, Melem (2,5,8-Triamino-tri-s-triazine), an important intermediate during condensation of melamine rings to graphitic carbon nitride: synthesis, structure determination by X-ray powder diffractometry, solid-state NMR and theoretical studies, J. Am. Chem. Soc. 125 (2003) 10288–10300.
[3] E. Kroke, M. Schwarz, E. Horath-Bordon, P. Kroll, B. Noll, A.D. Norman, Tri-s-triazine derivatives. Part I. From trichloro-tri-s-triazine to graphitic C_3N_4 structures, New J. Chem. 26 (2002) 508–512.
[4] A.H. Reshak, Thermoelectric properties for AA and AB stacking of carbon nitride polymorph (C_3N_4), RSC Adv. 4 (2014) 63137–63142.
[5] R. Huang, Graphene: show of adhesive strength, Nat. Nanotechnol. 6 (2011) 537–538.
[6] D.M. Teter, R.J. Hemley, Low-compressibility carbon nitrides, Science 271 (1996) 53–55.
[7] X. Li, Y. Dai, Y. Ma, S. Han, B. Huang, Graphene/g-C_3N_4 bilayer: considerable band gap opening and effective band structure engineering, Phys. Chem. Chem. Phys. 16 (2014) 4230–4234.
[8] Y. Zhang, T. Mori, J. Ye, Polymeric carbon nitrides: semiconducting properties and emerging applications in photocatalysis and photoelectrochemical energy conversion, Sci. Adv. Mater. 4 (2012) 282–291.
[9] Z. Tong, D. Yang, J. Shi, Y. Nan, Y. Sun, Z. Jiang, Three-dimensional porous aerogel constructed by g-C_3N_4 and graphene oxide nanosheets with excellent visible-light photocatlytic performance, ACS Appl. Mater. Interfaces 7 (2015) 25693–25701.
[10] J. Tian, Q. Liu, C. Ge, Z. Xing, A.M. Asiri, A.O. Al-Youbi, X. Sun, Ultrathin graphitic carbon nitride nanosheets: a low-cost, green, and highly efficient electrocatalyst toward the reduction of hydrogen peroxide and its glucose biosensing application, Nanoscale 5 (2013) 8921–8924.
[11] A.A.S. Nair, R. Sundara, N. Anitha, Hydrogen storage performance of palladium nanoparticles decorated graphitic carbon nitride, Int. J. Hydrogen Energy 40 (2015) 3259–3267.
[12] Y. Hou, J. Li, Z. Wen, S. Cui, C. Yuan, J. Chen, N-doped graphene/porous g-C_3N_4 nanosheets supported layered-MoS_2 hybrid as robust anode materials for lithium-ion batteries, Nano Energy 8 (2014) 157–164.
[13] G. Wu, N.H. Mack, W. Gao, S. Ma, R. Zhong, J. Han, J.K. Baldwin, P. Zelenay, Nitrogen-doped graphene-rich catalysts derived from heteroatom polymers for oxygen reduction in nonaqueous lithium-O_2 battery cathodes, ACS Nano 6 (2012) 9764–9776.
[14] Y. Zhang, T. Mori, J. Ye, Polymeric carbon nitrides: semiconducting properties and emerging applications in photocatalysis and photoelectrochemical energy conversion, Sci. Adv. Mater. 4 (2012) 1947–2935.
[15] Y. Fu, J. Zhu, C. Hu, X. Wu, X. Wang, Covalently coupled hybrid of graphitic carbon nitride with reduced graphene oxide as superior performance lithium-ion battery anode, Nanoscale 6 (2014) 12555–12564.
[16] P. Giannozzi, S. Baroni, N. Bonini, M. Calandra, R. Car, C. Cavazzoni, D. Ceresoli, G.L. Chiarotti, M. Cococcioni, I. Dabo, et al., QUANTUM ESPRESSO: a modular and open-source software project for quantum simulations of materials, J. Phys.: Condens. Matter 21 (2009) 395502–395521.
[17] J.P. Perdew, K. Burke, M. Ernzerhof, Generalized gradient approximation made simple, Phys. Rev. Lett. 77 (1996) 3865–3868.
[18] L. Kleinman, D.M. Bylander, Efficacious form for model pseudopotentials, Phys. Rev. Lett. 48 (1982) 1425–1428.
[19] H.J. Monkhorst, J.D. Pack, Special point for Brillouin-zone integrations, Phys. Rev. B 13 (1976) 5188–5192.
[20] D.R. Cooper, B. D'Anjou, N. Ghattamaneni, B. Harack, M. Hilke, A. Horth, N. Majlis, M. Massicotte, L. Vandsburger, E. Whiteway, V. Yu, Experimental review of graphene, international scholarly research network, ISRN Condens. Matter Phys. (2012), http://dx.doi.org/10.5402/2012/501686.
[21] N.W. Ashcroft, N.D. Mermin, Solid State Physics, Holt Rinehart and Winston, United States, 1976, p. 561 ff.
[22] C. Kittel, Introduction to Solid State Physics, John Wiley & Sons, Inc., United States of America, 2005.
[23] A. Cotton, G. Wilkinson, Advanced Inorganic Chemistry, John Wiley & Sons Inc., United States of America, 1972, p. 310 ff.
[24] P. Delhaes, Graphite and Precursors, CRC Press, 2001.
[25] C.B. Robledo, M.I. Rojas, O. Cámara, E.P.M. Leiva, First-principles studies concerning optimization of hydrogen storage in nanoporous reduced graphite oxide, Int. J. Hydrogen Energy 39 (2014) 4396–4403.
[26] A.Y. Liu, R.M. Wentzcovitch, Stability of carbon nitride solids, Phys. Rev. B: Solid State 50 (1994) 10362.
[27] http://www.crystalmaker.com/.
[28] http://crystalmaker.com/crystaldiffract/.
[29] http://crystalmaker.com/singlecrystal/.